T6SS translocates a micropeptide to suppress STING-mediated innate immunity by sequestering manganese

Lingfang Zhu[a,b,1], Lei Xu[a,1], Chenguang Wang[c,d,1], Changfu Li[a,b], Mengyuan Li[a], Qinmeng Liu[a], Xiao Wang[a], Wenhui Yang[e], Damin Pan[a], Lingfei Hu[e], Yadong Yang[a], Zhiqiang Lu[b], Yao Wang[a], Dongsheng Zhou[e,2], Zhengfan Jiang[c,d,2], and Xihui Shen[a,2]

[a]State Key Laboratory of Crop Stress Biology for Arid Areas, Shaanxi Key Laboratory of Agricultural and Environmental Microbiology, College of Life Sciences, Northwest A&F University, Shaanxi 712100, China; [b]Department of Entomology, College of Plant Protection, Northwest A&F University, Shaanxi 712100, China; [c]Key Laboratory of Cell Proliferation and Differentiation of the Ministry of Education, School of Life Sciences, Peking University, Beijing 100871, China; [d]Peking-Tsinghua Center for Life Sciences, Peking University, Beijing 100871, China; and [e]State Key Laboratory of Pathogen and Biosecurity, Beijing Institute of Microbiology and Epidemiology, Beijing 100071, China

Edited by Ralph R. Isberg, Tufts University School of Medicine, Boston, MA, and approved August 31, 2021 (received for review February 21, 2021)

Cellular ionic concentrations are a central factor orchestrating host innate immunity, but no pathogenic mechanism that perturbs host innate immunity by directly targeting metal ions has yet been described. Here, we report a unique virulence strategy of *Yersinia pseudotuberculosis* (*Yptb*) involving modulation of the availability of Mn^{2+}, an immunostimulatory metal ion in host cells. We showed that the *Yptb* type VI secretion system (T6SS) delivered a micropeptide, TssS, into host cells to enhance its virulence. The mutant strain lacking TssS (Δ*tssS*) showed substantially reduced virulence but induced a significantly stronger host innate immune response, indicating an antagonistic role of this effector in host antimicrobial immunity. Subsequent studies revealed that TssS is a Mn^{2+}-chelating protein and that its Mn^{2+}-chelating ability is essential for the disruption of host innate immunity. Moreover, we showed that Mn^{2+} enhances the host innate immune response to *Yptb* infection by activating the stimulator of interferon genes (STING)-mediated immune response. Furthermore, we demonstrated that TssS counteracted the cytoplasmic Mn^{2+} increase to inhibit the STING-mediated innate immune response by sequestering Mn^{2+}. Finally, TssS-mediated STING inhibition sabotaged bacterial clearance in vivo. These results reveal a previously unrecognized bacterial immune evasion strategy involving modulation of the bioavailability of intracellular metal ions and provide a perspective on the role of the T6SS in pathogenesis.

type VI secretion system (T6SS) | micropeptide | manganese | innate immunity | STING

The type VI secretion system (T6SS) is a widely distributed phage tail-like protein export apparatus that delivers effectors into neighboring cells (1, 2). While primarily recognized as a bacterial weapon for delivering a vast array of enzymatic effectors into targeted prokaryotic cells (3, 4), some T6SSs associated with pathogens are necessary for full virulence, as they inject anti-eukaryotic effectors into host cells that interact with the microtubule network, promote bacterial escape into the cytoplasm, and modulate host inflammation (5–9). To expand our understanding of the versatile T6SS nanomachine, the identification of more anti-eukaryotic T6SS effectors that promote bacterial virulence in eukaryotic cells is needed.

The T6SS is also involved in the acquisition of metal ions such as manganese (Mn^{2+}) through the release of metal-chelating effectors (10). Mn^{2+} is an essential micronutrient that serves as a cofactor for enzymes involved in intermediary metabolism and adaptation to oxidative stress (11). Mn^{2+} is also required by bacterial pathogens to establish an infective lifestyle within the host through the detoxification of reactive oxygen species released by immune cells (12). Recently, Wang et al. identified a novel role of Mn^{2+} in orchestrating host innate immune responses by acting as an activator of the cyclic GMP-AMP (cGAMP) synthase (cGAS)-stimulator of interferon genes (STING) pathway (13). Upon viral infection, Mn^{2+} is released from membrane-enclosed organelles into the cytosol, where it binds to cGAS to increase its enzymatic activity and sensitivity to double-stranded DNA. In addition, Mn^{2+} promotes STING activity by enhancing cGAMP–STING-binding affinity (13). This finding raises the question of whether metal-chelating T6SS effectors can be translocated into host cells to modulate the STING-mediated innate immune response by sequestering Mn^{2+}, thus acting as anti-eukaryotic effectors.

As a cytosolic pattern recognition receptor (PRR), cGAS is thought to be the main receptor that senses cytosolic DNA (14) and subsequently produces the second messenger 2′3′-cGAMP (15), which binds STING with high affinity and triggers its oligomerization and translocation (16). The activation of STING activates the kinase TBK1 that leads to phosphorylation of the transcription factor IRF3, which is dimerized and translocated

Significance

Although emerging evidence suggests that the STING-mediated immune response pathway plays a crucial role in microbial pathogen infection, few bacterial effectors have been reported to target this pathway. Here, we identified a T6SS-secreted micropeptide, TssS, which is crucial for the pathogenesis of *Yptb*. Distinct from traditional bacterial effectors that target host proteins or other macromolecules, TssS inhibits STING oligomerization and downstream signaling pathways by chelating Mn^{2+}. Thus, TssS mediates a previously unrecognized immune evasion mechanism by modulating the availability of immunostimulatory Mn^{2+} in host cells. This finding reveals a strategy to modulate the STING pathway by microbial pathogens, provides a new perspective on the role of T6SS in pathogenesis, and highlights the importance of micropeptides in pathogen–host interactions.

Author contributions: D.Z., Z.J., and X.S. designed research; L.Z., L.X., C.W., M.L., Q.L., X.W., and Y.Y. performed research; C.W., W.Y., D.P., L.H., Z.L., Y.W., and X.S. contributed new reagents/analytic tools; L.Z., L.X., C.W., C.L., Z.L., Y.W., and X.S. analyzed data; and L.Z., L.X., D.Z., Z.J., and X.S. wrote the paper.

The authors declare no competing interest.

This article is a PNAS Direct Submission.

[1]L.Z., L.X., and C.W. contributed equally to this work.

[2]To whom correspondence may be addressed. Email: xihuishen@nwsuaf.edu.cn, jiangzf@pku.edu.cn, or dongshengzhou1977@gmail.com.

This article contains supporting information online at http://www.pnas.org/lookup/suppl/doi:10.1073/pnas.2103526118/-/DCSupplemental.

Published October 8, 2021.

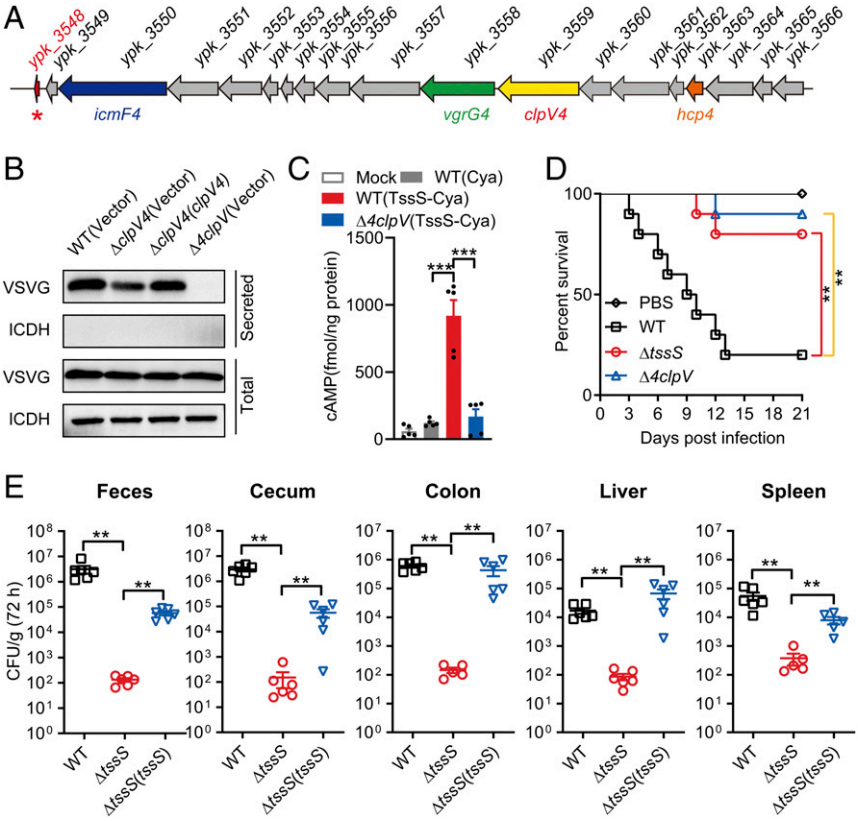

Fig. 1. A T6SS-secreted micropeptide contributes to *Yptb* virulence. (*A*) Structure of the *Yptb* T6SS4 gene cluster. The *tssS* gene (*ypk_3548*) is indicated with a red asterisk. (*B*) TssS is a T6SS4 effector. An immunoblot analysis of vesicular stomatitis viral glycoprotein (VSVG)-tagged TssS protein levels in culture supernatant of the relevant *Yptb* strains is shown. The cytoplasmic protein isocitrate dehydrogenase (ICDH) was used as a loading control and lysis control for the total and secreted fractions. (*C*) Raw264.7 cells were mock infected or infected with indicated *Yptb* strains expressing Cya-fused TssS at a multiplicity of infection of 20 for 2 h. Cyclic AMP present in lysates was measured. (*D*) C57BL/6 mice were intragastrically inoculated with *Yptb* WT, Δ*4clpV*, or Δ*tssS*. The survival rate of the mice was determined. (*E*) C57BL/6 mice were intragastrically inoculated with *Yptb* WT, Δ*tssS*, or Δ*tssS*(*tssS*). Homogenates of different tissues were plated to determine the bacterial CFU count per gram of organs at 72 h postinfection. Error bars represent ± SEM; $^{**}P < 0.01$; $^{***}P < 0.001$.

to the nucleus to induce the expression of type I interferons (IFNs) and IFN-stimulated genes (ISGs) (17). In addition to 2′3′-cGAMP, STING can also recognize bacterial cyclic dinucleotides such as cyclic dimeric guanosine monophosphate (c-di-GMP) (18), cyclic dimeric adenosine monophosphate (c-di-AMP) (19), and 3′3′-cGAMP (20), ubiquitous bacterial second messengers. Primarily identified as a direct sensor of cyclic dinucleotides (18, 19), the function of the STING pathway has been extensively studied in the context of microbial infections, autoinflammatory diseases, cancer, and other sterile inflammations (21–23). However, the role of STING in host immune response against bacterial infection remains controversial (24).

While studies on *Yersinia* outer proteins (Yops) secreted by the type III secretion system (T3SS) have provided tremendous information about bacterial pathogenic strategies (25–27), the role of *Yersinia* T6SS effectors in regulating the host cellular response remains largely unknown, despite the identification of four T6SS gene clusters in *Yersinia pseudotuberculosis* (*Yptb*) (28, 29). Here, we identified a T6SS-secreted micropeptide, TssS (T6SS-secreted micropeptide suppressing STING), which plays crucial roles in the pathogenesis of *Yptb*. Mechanistically, TssS deploys a unique virulence strategy by sequestering immunologically active Mn^{2+} in the host cell, antagonizing the STING-mediated innate immune response.

Results

A Micropeptide Translocated by the T6SS Contributes to *Yptb* Virulence. Previously, it was reported that the *Yptb* T6SS4 functions in resistance to oxidative stress and host nutritional immunity by secreting a zinc-binding effector, YezP (YPK_3549), which is located near the end of the T6SS4 gene cluster (30). Interestingly, immediately downstream of the YPK_3549 ORF is a 48-residue micropeptide encoding ORF (YPK_3548, hereafter referred to as TssS) that is transcribed in the same direction as those of the T6SS4 genes, suggesting that this gene is part of the T6SS4 operon (Fig. 1*A* and *SI Appendix*, Fig. S1*A*).

We first examined whether the TssS micropeptide is a T6SS-secreted effector like YezP. As shown in Fig. 1*B*, while significant amounts of TssS could be readily detected in the culture supernatant of *Yptb* wild-type (WT) culture, its secretion was substantially abrogated in the Δ*clpV4* mutant and could be rescued to the WT level through complementation. The residual secretion exhibited by the Δ*clpV4* mutant indicates potential cross-recognition of this effector by other T6SSs, as TssS secretion was completely abrogated in the Δ4*clpV* mutant (a mutant defective in all four T6SSs, *SI Appendix*, Fig. S1*B*), and complementation with any *clpV* gene only partially restored its secretion (*SI Appendix*, Fig. S1*B*). Notably, complementation of the *clpV4* gene rescued TssS secretion to a large extent, suggesting that TssS is a substrate mainly secreted by T6SS4, although it can also be secreted by other T6SSs. This notion was further substantiated by the finding that TssS binds directly to Hcp4 (*SI Appendix*, Fig. S1*C*), the T6SS component that acts as a carrier protein for the secretion of multiple T6SS effectors (31).

To examine whether TssS is translocated into the cytosol of mammalian cells by the T6SS, the *Bordetella pertussis* cyclic AMP (cAMP) synthetase (Cya) reporter assay was employed in which the TssS-Cya fusion protein requires the cofactor calmodulin, which is only present in the cytosol of eukaryotic cells (32). Thus, intracellular cAMP levels could reflect intracellular translocation of the TssS-Cya fusion protein. As expected, high levels of intracellular cAMP were detected only in cells infected with the *Yptb* WT strain expressing TssS-Cya but not in those infected with the Δ*4clpV* mutant strain that expresses TssS-Cya (Fig. 1*C*), indicating that TssS is translocated into host cells during *Yptb* infection in a T6SS-dependent manner. The translocation of TssS into mammalian cells was confirmed using the TEM1 (β-lactamase) assay by fusing the TEM1 reporter

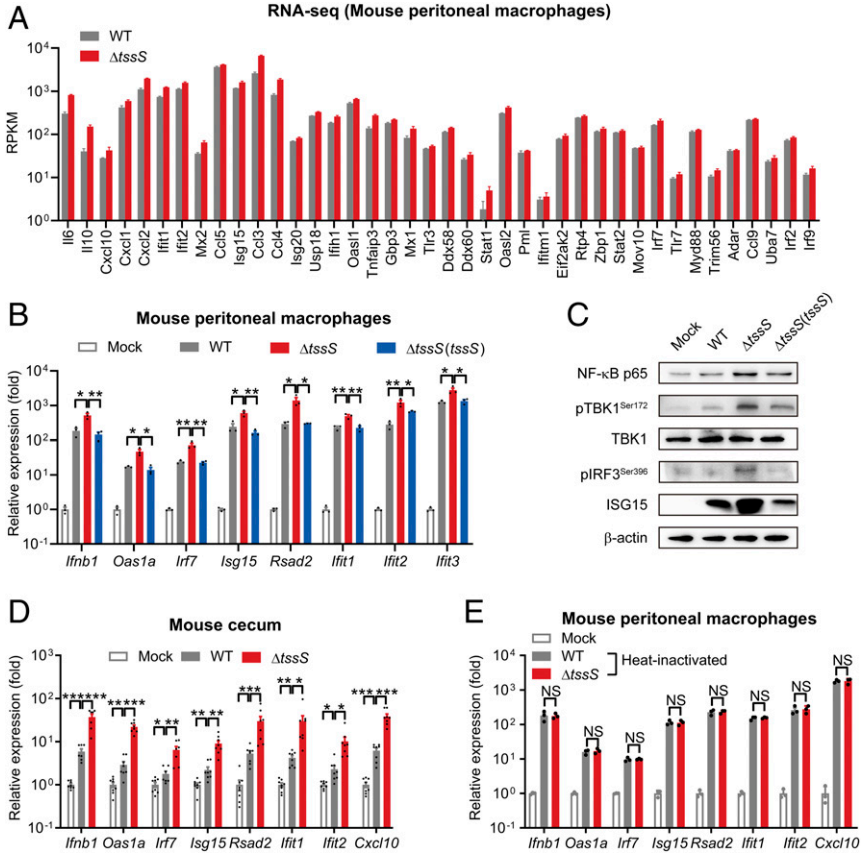

Fig. 2. TssS inhibits the host innate immune response. (*A*) RNA-seq results of different ISGs of mouse PMs infected with *Yptb* WT or Δ*tssS*. RPKM: reads per kilobase of exon model per million mapped reads. (*B*) qRT-PCR analysis of the gene expression in PMs infected with *Yptb* WT, Δ*tssS*, or Δ*tssS*(*tssS*). (*C*) Immunoblot analysis of the protein expression in PMs infected with *Yptb* WT, Δ*tssS*, or Δ*tssS*(*tssS*). (*D*) qRT-PCR analysis of gene expression in the cecum of C57BL/6 mice mock infected or infected intragastrically with *Yptb* WT or Δ*tssS* for 72 h. (*E*) qRT-PCR analysis of gene expression in PMs infected with heat-inactivated strains. Data in *B*, *D*, and *E* were normalized to mock-infected control (Mock, set as 1), and *Gapdh* was used as the housekeeping gene. Error bars represent ± SEM; $*P < 0.05$; $**P < 0.01$; $***P < 0.001$; NS, not significant.

protein to the C terminus of TssS. The T6SS-dependent translocation of TssS into HeLa cells was determined by fluorescence resonance energy transfer using the β-lactamase cleavable substrate CCF2/AM, which, upon excitation at 409 nm, emits green fluorescence (520 nm) in the absence of β-lactamase and emits blue fluorescence (447 nm) in the presence of β-lactamase (9). Consistently, fluorescence microscopy revealed that the cells showed blue fluorescence upon infection with the WT strain expressing TssS-TEM1 but exhibited green fluorescence after infection with the Δ*4clpV* mutant expressing TssS-TEM1 (*SI Appendix*, Fig. S1*D*).

The finding that TssS is translocated into mammalian cells indicated the role of TssS in *Yptb* virulence. To explore this possible association, *Yptb* WT, Δ*tssS*, and Δ*4clpV* were intragastrically inoculated into C57BL/6 mice, and the survival rates of each group were analyzed. The results showed that infection with the WT strain led to more than 80% death within 2 wk of infection. Surprisingly, significantly fewer mice were dead in the Δ*tssS* mutant-infected group (Fig. 1*D*). These results indicated that the TssS micropeptide is vital to the virulence of *Yptb*. A slightly higher survival rate was observed in the Δ*4clpV* mutant-infected mice, suggesting that other T6SS effectors contribute to the virulence of *Yptb* (30). Next, the bacterial loads recovered from the cecum, feces, colon, liver, and spleen were counted at 72 h postinfection with *Yptb*. Consistently, mice infected with Δ*tssS* had significantly fewer colony-forming units (CFU) per gram of tissue compared to WT-infected mice. Moreover, the complementation of *tssS* significantly restored the bacterial loads of the Δ*tssS* mutant in various tissues (Fig. 1*E*). Together, we characterized a T6SS-secreted micropeptide that plays crucial roles in the virulence of *Yptb*.

TssS Inhibits the Host Innate Immune Response. To the best of our knowledge, no small bacterial effector (less than 48 amino acid [aa]) has been reported to play an important role in bacterial virulence. Therefore, we performed transcriptomic analysis using RNA sequencing (RNA-seq) to identify differentially expressed host genes upon WT and Δ*tssS* infection. We found that immune system and signal transduction pathways were differentially induced between Δ*tssS* and WT infection in mouse peritoneal macrophages (PMs) (*SI Appendix*, Fig. S2*A*). Gene set enrichment analysis results showed that many of these differentially induced genes belong to IFN- and STING-related signaling pathways (*SI Appendix*, Fig. S2*B*). Specifically, many ISGs were induced preferentially by Δ*tssS* in PMs (Fig. 2*A*). To validate the RNA-seq results, the expression of many ISGs including type I IFN *Ifnb1* and the IRF3-responsive genes *Rsad2*, *Isg15*, *Ifit1*, *Irf7*, and *Ifit2* was measured (13). Consistently, compared to infection with the WT strain, Δ*tssS* infection provoked higher expression levels of these genes in mouse PMs (Fig. 2 *B* and *C*). In particular, the expression of *Ifnb1* and IRF3-responsive genes was elevated in Δ*tssS*-infected cells (Fig. 2*B*). Moreover, the phosphorylation of IRF3 and TBK1, hallmarks of IFN-related innate immune activation, and the protein expression of the IRF3-responsive gene ISG15 were more strongly induced by Δ*tssS* infection (Fig. 2*C*), suggesting that TssS inhibits the *Yptb*-induced IFN-related host innate immune response. Notably, ISG expression was comparable upon infection with the WT and the complemented strain Δ*tssS*(*tssS*), further corroborating the role of TssS in regulating host innate immunity (Fig. 2 *B* and *C*). Similarly, qRT-PCR results obtained from the cecum of infected mice confirmed that numerous ISGs were elicited at higher levels in Δ*tssS*-infected mice (Fig. 2*D*), despite fewer bacteria being recovered from their cecum (Fig. 1*E*). Together, these results indicated that TssS is important for inhibiting *Yptb*-elicited innate immunity.

Notably, the lipopolysaccharide (LPS) content in the Δ*tssS* mutant was the same as that in the WT strain (*SI Appendix*, Fig. S2*C*), indicating that different innate immune responses induced by WT and Δ*tssS* were not due to different LPS content. In addition, the difference in capacity to induce ISGs was not due to the growth advantage of Δ*tssS*, as it had a similar growth curve to WT in *Yersinia* lysogeny broth (YLB) medium (*SI Appendix*, Fig. S2*D*) and attenuated growth ability in Raw264.7 cells (*SI Appendix*, Fig. S2*E*). To further explore the role of TssS in the *Yptb*-induced innate immune response, we inactivated both the WT and Δ*tssS* strains through heating or ultraviolet (UV) irradiation to eliminate the active secretion of bacterial effectors and used the inactivated bacterial cells to treat PMs. Similar ISG expression patterns were elicited by these inactivated strains, indicating that a secreted and functional TssS protein is essential to the observed inhibition (Fig. 2*E* and *SI Appendix*, Fig. S2*F*). Together, these results demonstrated that TssS plays crucial roles in suppressing the *Yptb*-induced host innate immune response.

TssS Is a Mn^{2+}-Binding Effector, and Its Mn^{2+}-Binding Activity Is Required for *Yptb* Virulence. Recently, the T6SS4 of *Burkholderia thailandensis* was reported to be critical for combating oxidative stress by importing Mn^{2+} (10). Given the high similarity of their operon structures (Fig. 1*A* and *SI Appendix*, Fig. S3), we speculated that the T6SS4 of *Yptb* might also be involved in Mn^{2+} acquisition. Indeed, the survival of bacteria under oxidative stress and intracellular Mn^{2+} levels were both significantly reduced in the Δ*clpV4* mutant (*SI Appendix*, Fig. S4 *A* and *B*), indicating that *Yptb* T6SS4 has the capacity for Mn^{2+} uptake to combat oxidative stress.

Previous research showed that *B. thailandensis* T6SS4 secreted a Mn^{2+}-binding effector TseM (BTH_II1883, 141 aa), which is located at the end of the T6SS4 gene cluster, for importing Mn^{2+} (10). Speculatively, it is highly likely that TssS, which is located at the end of the T6SS4 gene cluster in *Yptb*, is also a Mn^{2+}-binding protein, although no sequence similarity was found between these proteins. To experimentally assess the Mn^{2+}-binding potential of TssS, atomic absorption spectrometry analysis was employed, which showed that purified recombinant TssS could specifically bind Mn^{2+} but not Ca^{2+}, Mg^{2+}, or Zn^{2+} (Fig. 3*A*). A binding K_d (6.83 μM) comparable to that of TseM (2.87 μM) was obtained through isothermal titration calorimetry (ITC) (Fig. 3*B*). The mutation of Glu30, Glu36, His43, and Gln44 ($TssS^{E30A/E36A/H43A/Q44A}$, TssS*) (*SI Appendix*, Fig. S4*C*), residues predicted to be crucial for Mn^{2+}-binding proteins (33–35), dramatically reduced the binding affinity of TssS for Mn^{2+} (K_d = 165.2 μM) (Fig. 3*B*). Notably, the TssS* protein exhibited similar properties to TssS in protein expression, secretion, and stability (*SI Appendix*, Fig. S4 *D–G*). Consistent with the report that TseM is required for T6SS-dependent Mn^{2+} acquisition under oxidative stress in *B. thailandensis*, deletion of *tssS* in *Yptb* markedly reduced intracellular Mn^{2+} accumulation under oxidative stress conditions, and complementation of the *tssS* gene restored intracellular Mn^{2+} to the WT level (Fig. 3*C*). However, deletion of *tssS* did not affect the accumulation of Fe, Mg, or Ca ions under the same conditions (*SI Appendix*, Fig. S4*H*). These results confirmed that TssS is an Mn^{2+}-binding protein involved in Mn^{2+} acquisition.

As an Mn-binding effector of oxidative stress-resistant T6SS4, TssS is expected to be necessary for maximizing bacterial survival under conditions of oxidative stress. Indeed, Δ*tssS* exhibited a significantly lower survival rate under oxidative stress, and this sensitivity could be restored to the WT level through complementation with the *tssS* gene but not with the Mn^{2+}-binding–defective *tssS** mutant gene (Fig. 3*D*). To further explore whether the Mn^{2+}-binding potential is required for TssS to exert its immunoregulatory function, we generated two complemented strains (Δ*tssS-tssS* and Δ*tssS-tssS**) by knock-in of the WT *tssS* or the Mn^{2+}-binding–defective mutant gene *tssS**, respectively, at the original site on the Δ*tssS* chromosome. As shown in Fig. 3*E*, significantly fewer bacteria were recovered from mice infected with the Δ*tssS-tssS** strain than from mice infected with Δ*tssS-tssS*, indicating that the Mn^{2+}-binding ability of TssS is crucial for its function in bacterial virulence. Indeed, the bacterial burdens were comparable between Δ*tssS*-infected and Δ*tssS-tssS**–infected mice. Notably, the growth ability of the Δ*tssS-tssS** strain in PMs was similar to that of the Δ*tssS* mutant (*SI Appendix*, Fig. S4*I*). In addition, the ISG expression induced by Δ*tssS-tssS** infection was also comparable to that induced by the Δ*tssS* strain (Fig. 3*F*). These results indicated that infection with the Mn^{2+}-binding–defective strain Δ*tssS-tssS** phenocopied Δ*tssS* mutant infection, suggesting that TssS requires its Mn^{2+}-binding ability to function in bacterial virulence and innate immune regulation.

Mn^{2+} Primes the Host Defense against *Yptb* Infection via the STING Pathway. Mn^{2+} enhances antiviral innate immunity by potentiating the cGAS-STING pathway (13). However, the protective role of Mn^{2+} against bacterial infection remains unknown. Therefore, we pretreated mice with $MnCl_2$ (25 mg · kg^{-1}) and infected them intragastrically with the *Yptb* WT strain. The results showed that Mn^{2+} pretreatment significantly increased the survival of mice infected with *Yptb* WT (Fig. 4*A*). Correspondingly, mice pretreated with Mn^{2+} had significantly fewer CFU per gram of tissue (cecum, feces, colon, liver, and spleen) compared to untreated mice (Fig. 4*B*). In addition, in *Yptb*-infected PMs, Mn^{2+} pretreatment significantly enhanced the gene expression of type I IFN *Ifnb1* and IRF3-responsive genes *Rsad2*, *Isg15*, and *Ifit1* (Fig. 4*C*). Consistently, Mn^{2+} pretreatment significantly increased *Yptb*-activated ISG15 and IFIT2 expression at the protein level (Fig. 4*D*). In particular, *Yptb* infection–induced phosphorylation of IRF3 and TBK1, hallmarks of STING-mediated immune response activation, was strongly potentiated by Mn^{2+} pretreatment (Fig. 4*D*), suggesting that Mn^{2+} enhances the STING-mediated host innate immune response. Moreover, Δ*tssS* infection–induced higher ISG expression was further enhanced with Mn^{2+} pretreatment (*SI Appendix*, Fig. S5 *A* and *B*). Previous research characterized c-di-GMP as a pathogen-associated molecular pattern that could activate the host immune response through direct binding to STING (18). Interestingly, the c-di-GMP–induced ISG expression in bone marrow–derived macrophages (BMDMs) was further potentiated by Mn^{2+} treatment (*SI Appendix*, Fig. S5*C*).

To further assess the physiological significance of Mn^{2+} in defending against *Yptb* infection, weaned mice were fed ad libitum with an Mn-deficient diet for 6 wk to generate Mn-deficient mice as described (13). Mn-deficient mice were intragastrically infected with the *Yptb* WT strain. The bacterial loads of Mn-deficient mice were significantly higher than those of control mice at 72 h postinfection (*SI Appendix*, Fig. S5*D*). We next evaluated the cellular immune response to bacterial infection under Mn^{2+}-deficient conditions. PMs from Mn^{2+}-deficient mice were cultured in serum-free optimized minimal essential medium, which contains an untraceable level of Mn^{2+}. The ISG expression in these Mn-deficient macrophages against *Yptb* infection was significantly attenuated (*SI Appendix*, Fig. S5*E*). Consistently, the cellular responses to c-di-GMP were also significantly attenuated in Mn^{2+}-deficient macrophages (*SI Appendix*, Fig. S5*F*). Together, these results indicated that Mn^{2+} is important for host defense against *Yptb* infection.

To test directly whether Mn^{2+} protected the host from *Yptb* infection via STING, C57BL/6 or STING-deficient ($Tmem173^{-/-}$) mice were pretreated with $MnCl_2$, and bacterial burdens in mice were measured 72 h postinfection. Although

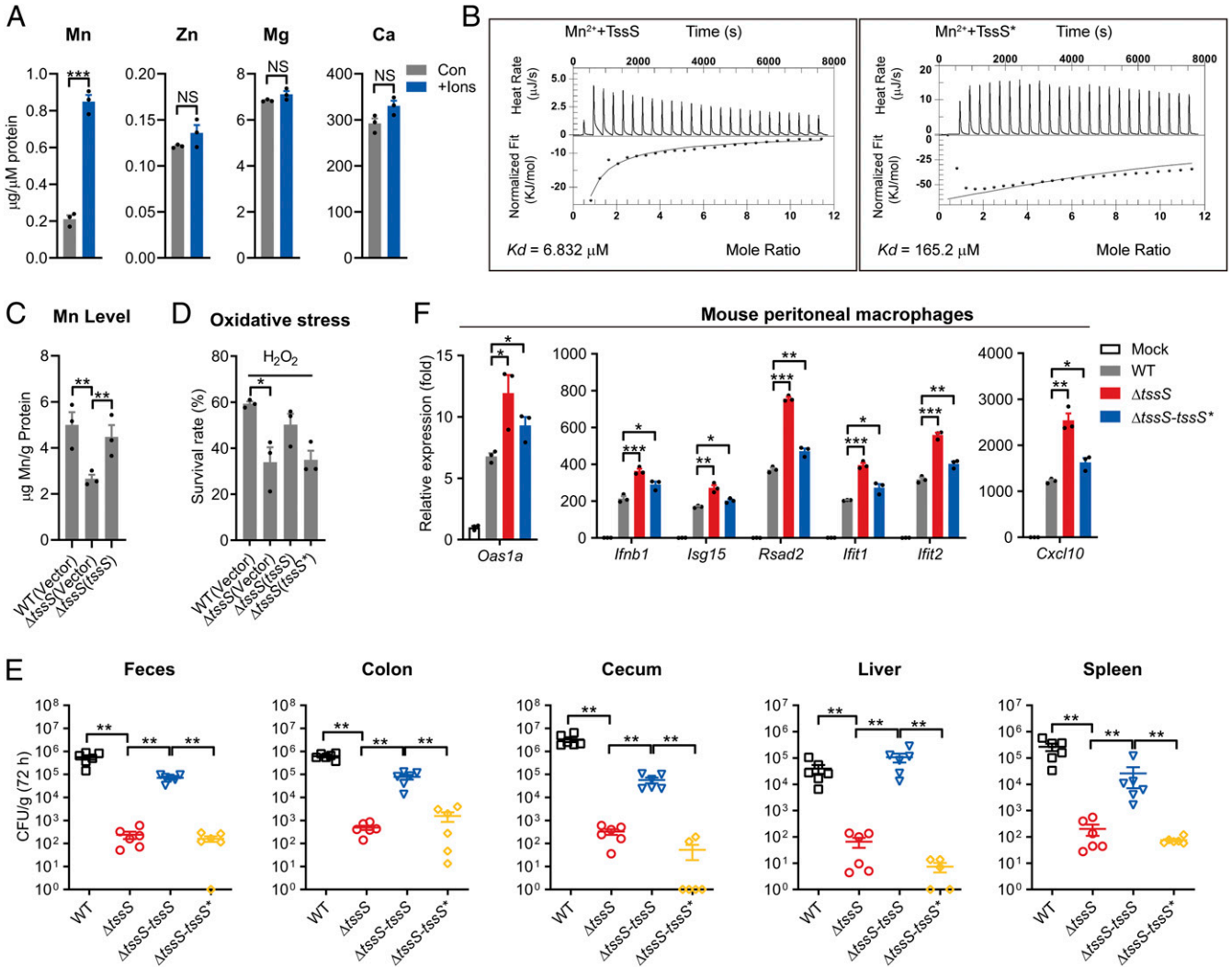

Fig. 3. TssS is a Mn^{2+}-binding micropeptide, and its Mn^{2+}-binding activity is required for *Yptb* virulence. (*A*) The binding of divalent ions by TssS was detected by atomic adsorption spectrometry. (*B*) The binding of Mn^{2+} with Mn^{2+}-free TssS protein or TssS* ($TssS^{E30A/E36A/H43A/Q44A}$ mutated protein) was determined via ITC. (*C*) Stationary-phase *Yptb* WT, Δ*tssS*, mutant and Δ*tssS*(*tssS*) were exposed to 2.5 mM H_2O_2 for 40 min in M9 medium with 1 μM $MnSO_4$. Mn^{2+} associated with bacterial cells was measured by ICP-MS. (*D*) The viability of *Yptb* strains under oxidative stress was determined. *Yptb* WT, Δ*tssS*, Δ*tssS*(*tssS*), and Δ*tssS*(*tssS**) were exposed to H_2O_2 (1 mM) for 40 min in M9 medium. (*E*) C57BL/6 mice were intragastrically inoculated with the *Yptb* WT, Δ*tssS*, Δ*tssS-tssS*, or Δ*tssS-tssS**, respectively. Homogenates of different tissues were plated to determine the bacterial CFU counts per gram of organs at 72 h postinfection. (*F*) qRT-PCR analysis of the gene expression in PMs infected with *Yptb* WT, Δ*tssS*, Δ*tssS-tssS*, or Δ*tssS-tssS**, respectively. Data in *F* were normalized to mock-infected control (Mock, set as 1), and *Gapdh* was used as the housekeeping gene. Error bars represent ± SEM; $*P < 0.05$; $**P < 0.01$; $***P < 0.001$; NS, not significant.

Mn^{2+} pretreatment significantly reduced the bacterial burdens in the feces and cecum of C57BL/6 mice, this effect was not observed in *Tmem173*$^{-/-}$ mice (Fig. 4*E*). Similar results were obtained by infection of Mn^{2+}-deficient C57BL/6 or *Tmem173*$^{-/-}$ mice. Although Mn^{2+}-deficient C57BL/6 mice showed dramatically increased bacterial burdens compared to control C57BL/6 mice, no increase in CFU count was observed in the feces and cecum of Mn^{2+}-deficient *Tmem173*$^{-/-}$ mice compared to control *Tmem173*$^{-/-}$ mice (*SI Appendix*, Fig. S5*G*). Therefore, consistent with its role in antiviral innate immunity, Mn^{2+} protected the host from *Yptb* infection in a manner involving STING.

In mammalian cells, most cellular Mn^{2+} is found in membrane-enclosed organelles. Upon viral infection, Mn^{2+} is released into the cytosol to enhance antiviral innate immunity (13, 36). As Mn^{2+} is also required for defense against *Yptb* infection, we explored whether bacterial infection could also induce Mn^{2+} release into the cytosol. Direct measurement of intracellular Mn^{2+} concentrations in the host cytosol upon *Yptb* infection is impractical due to technical challenges, and therefore, we measured intracellular Mn^{2+} concentrations following treatment of Raw264.7 cells with LPS, the major innate immune activator in gram-negative bacteria. We found that cells stimulated with LPS exhibited much higher cytosolic (S100) Mn levels compared to untreated cells, probably due to LPS-induced mitochondrial membrane potential disruption (37–39), which causes Mn to escape from mitochondria (13, 40). Correspondingly, the Mn level in the membrane fraction (pellet) was reduced in LPS-treated cells (Fig. 4*F*). Consistent with previous reports, the cytoplasmic Zn level was also sharply elevated upon LPS stimulation (41, 42), while the Ca and Mg levels were not affected (*SI Appendix*, Fig. S5*H*). These results indicated that, similar to viral infection, bacterial infection could induce Mn^{2+} release into the cytosol to enhance the

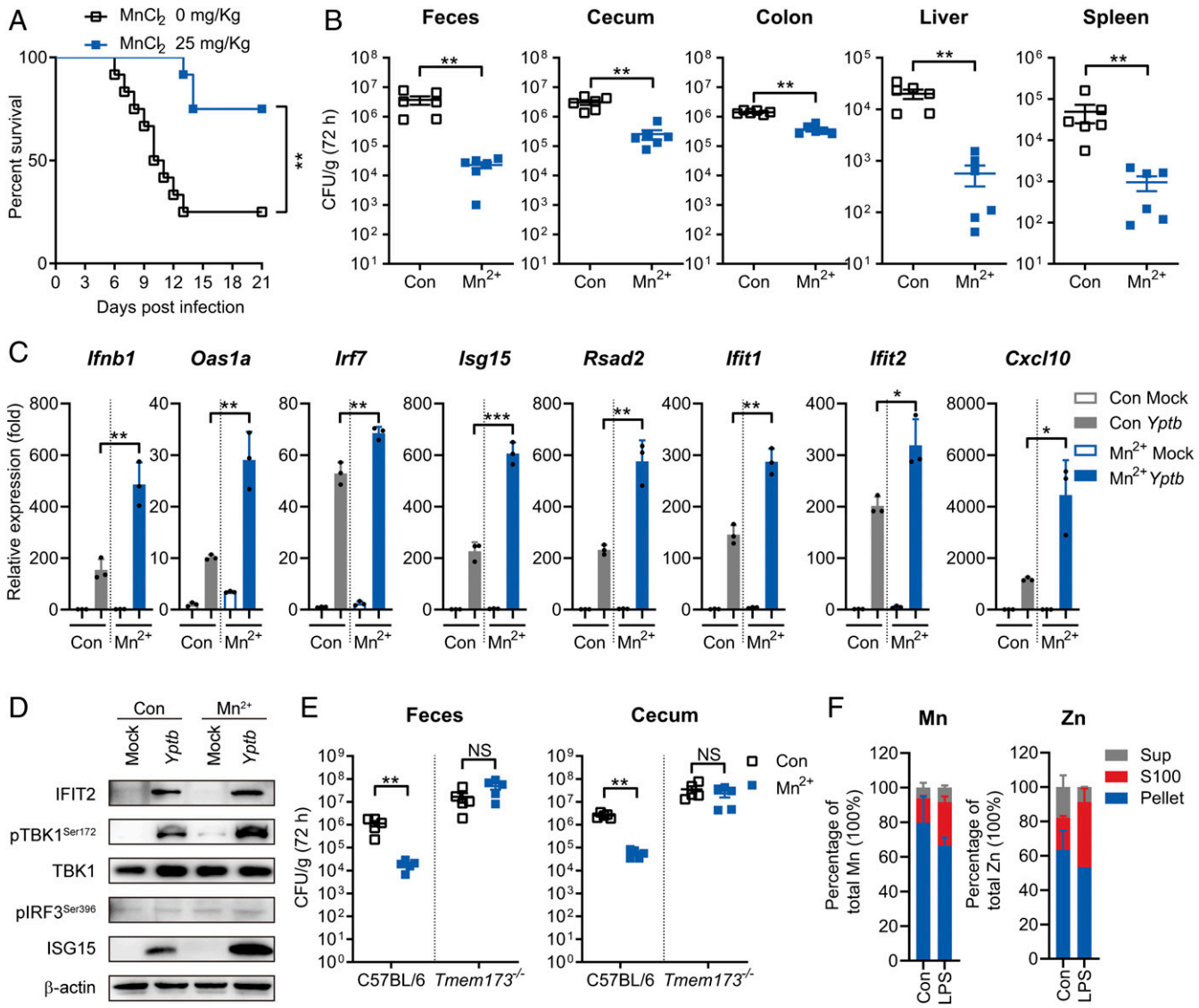

Fig. 4. Mn^{2+} primes the antimicrobial immune response via STING. (*A* and *B*) C57BL/6 mice were pretreated with or without $MnCl_2$ (25 mg · kg^{-1}) intraperitoneally for 24 h and were intragastrically inoculated with *Yptb* WT. (*A*) The survival rate of the mice was determined. (*B*) Homogenates of different tissues were plated to determine the bacterial CFU counts per gram in the indicated organs of the untreated (Con) or Mn^{2+}-treated (Mn^{2+}) mice at 72 h postinfection. (*C* and *D*) qRT-PCR analysis of the gene expression (*C*) and immunoblot analysis of the protein (*D*) in PMs untreated (Con) or pretreated with 100 μM $MnCl_2$ (Mn^{2+}) for 24 h and mock infected (Mock) or infected with *Yptb* WT. (*E*) C57BL/6 or *Tmem173*$^{-/-}$ mice were untreated (Con) or pretreated with $MnCl_2$ (25 mg · kg^{-1}) (Mn^{2+}) intravenously for 24 h and intragastrically inoculated with *Yptb* WT. Homogenates of feces and cecum were plated to determine the bacterial CFU numbers per gram of organs at 72 h postinfection. (*F*) Mn and Zn concentrations in the indicated cellular components and culture medium (Sup). Raw264.7 cells were untreated (Con) or treated with LPS (4 μg · mL^{-1}). Data in *C* were normalized to untreated, mock-infected control (Con Mock, set as 1). *Gapdh* was used as the housekeeping gene. Error bars represent ± SEM; $*P < 0.05$; $**P < 0.01$; $***P < 0.001$; NS, not significant.

STING-mediated immune response, which is important for host defense against *Yptb* infection.

TssS Inhibits STING Activity to Regulate Host Innate Immune Responses. We have shown that TssS is a Mn^{2+}-chelating anti-eukaryotic T6SS effector that inhibits host innate immunity (Figs. 1–3) and that Mn^{2+} strongly potentiates the innate immune response via the STING-mediated pathway (Fig. 4). These findings prompted us to further investigate whether the Mn^{2+}-chelating TssS inhibits Mn^{2+}-enhanced STING activation. First, we employed 2′3′-cGAMP and c-di-GMP to activate STING and its downstream pathways in PMs. Both 2′3′-cGAMP and c-di-GMP induced expression of a wide range of ISGs, and Mn^{2+} strongly potentiated their expression levels. Interestingly, the overexpression of TssS in macrophages significantly blocked the 2′3′-cGAMP– and c-di-GMP–induced Mn^{2+}-enhanced expression of ISGs, suggesting that TssS inhibits Mn^{2+}-enhanced STING activation (Fig. 5*A* and *B*). Similar results were obtained by the addition of purified TssS proteins into the medium (*SI Appendix*, Fig. S6 *A* and *B*). Next, we explored whether TssS could inhibit STING activity by testing STING oligomerization, the hallmark of STING activation (16). As shown in Fig. 5*C*, STING oligomerization in 293T cells induced by c-di-GMP and Mn^{2+} was greatly reduced by the addition of TssS protein but not the Mn^{2+}-binding–defective TssS* protein.

To further elucidate the role of STING in TssS-mediated innate immune suppression, BMDMs derived from C57BL/6 or

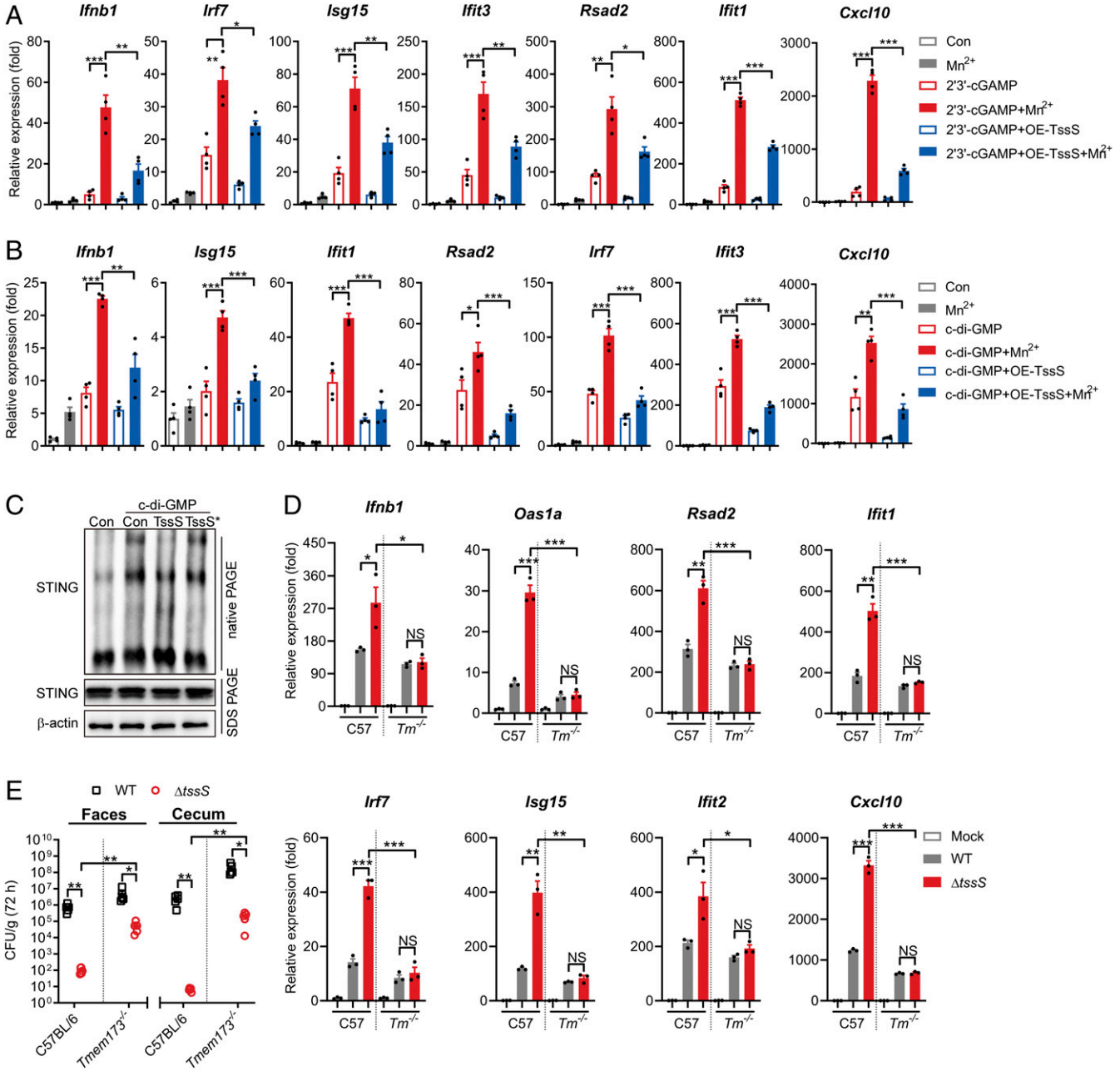

Fig. 5. TssS inhibits STING activity to suppress host innate immune responses. (*A* and *B*) PMs were transduced with the pSIN-IRES-Puro-4×*tssS* overexpression vector. At 24 h post-transduction, the cells were pretreated with or without 100 μM $MnCl_2$ for 24 h. At 48 h post-transduction, cells were lipofectamine transfected with 4 μM 2′3′-cGAMP (*A*) or 20 μM c-di-GMP (*B*). Gene expression of ISGs were determined at 4 h post c-di-GMP or 2′3′-cGAMP transfection. (*C*) 293T cells were transfected with STING-Flag plasmid. Cells were further untreated (Con) or pretreated with 100 μM $MnCl_2$ and along with or without 10 μM TssS or TssS* protein for 24 h and then lipofectamine transfected with 20 μM c-di-GMP. Cell lysates were immunoblotted with an antibody against STING after sodium dodecyl sulfate–polyacrylamide gel electrophoresis (PAGE) and native PAGE. (*D*) qRT-PCR analysis of gene expression in C57BL/6 or *Tmem173*$^{-/-}$ PMs mock infected or infected with the *Yptb* WT or Δ*tssS* strain. (*E*) C57BL/6 or *Tmem173*$^{-/-}$ mice were intragastrically inoculated with *Yptb* WT or Δ*tssS*. Homogenates of different tissues were plated to determine the bacterial CFU numbers per gram of organs at 72 h postinfection. Data in *A* and *B* were normalized to untreated control (Con, set as 1). Data in *D* were normalized to mock-infected C57BL/6 PMs and mock-infected *Tmem173*$^{-/-}$ PMs, respectively (Mock, both set as 1). *Gapdh* was used as the housekeeping gene. Error bars represent ± SEM; **P* < 0.05; ***P* < 0.01; ****P* < 0.001; NS, not significant.

STING-deficient *Tmem173*$^{-/-}$ mice were infected with the WT or Δ*tssS* mutant. As shown in Fig. 5*D*, the Δ*tssS* mutant induced significantly higher levels of ISG expression than the *Yptb* WT strain did in C57BL/6 cells, while no significant differences were detected in *Tmem173*$^{-/-}$ cells infected with *Yptb* WT and Δ*tssS*. Notably, a slightly but significantly decreased level of ISG expression was detected in *Yptb* WT-infected STING-deficient cells compared to that in C57BL/6-derived BMDMs. These results indicated that TssS inhibits host innate immune response via STING.

To directly confirm that TssS suppresses the host innate immune response through STING, we used the *Yptb* WT and Δ*tssS* strains to infect C57BL/6 or *Tmem173*$^{-/-}$ mice. In C57BL/6 mice, the bacterial burden of the WT strain was

significantly higher (three logs in feces and five logs in cecum) than that of the Δ*tssS* mutant in the feces and cecum (Fig. 1*E* and 5*E*). In contrast, the differences in bacterial burden between WT and Δ*tssS* were significantly attenuated in *Tmem173*$^{-/-}$ mice (two logs in feces and three logs in cecum) (Fig. 5*E*). Of note, higher bacterial burdens were obtained from the feces and cecum in Δ*tssS*-infected *Tmem173*$^{-/-}$ mice than in those of Δ*tssS*-infected C57BL/6 mice (Fig. 5*E*). To exclude the role of TssS-mediated interbacterial competition in possibly affecting the *Yersinia* bacterial burden in mouse gut, we treated C57BL/6 and *Tmem173*$^{-/-}$ mice with an antibiotics mixture to eliminate the gut microbiome followed by intragastrical infection with *Yptb* WT or Δ*tssS*. As shown in *SI Appendix*, Fig. S6*C*, bacterial burden in Δ*tssS*-infected C57BL/6 mice is significantly lower than that in *Yptb* WT-infected mice. However, the differences in bacterial burden between WT and Δ*tssS* were strongly attenuated in *Tmem173*$^{-/-}$ mice. Similar results were obtained by intraperitoneal infection of C57BL/6 or *Tmem173*$^{-/-}$ mice with *Yptb* WT or Δ*tssS* (*SI Appendix*, Fig. S6*D*). Taken together, these results demonstrated that the T6SS effector TssS robustly inhibits STING activation, thereby inhibiting its downstream pathway and subverting the host innate immune response.

TssS Suppresses the STING-Mediated Innate Immune Response by Sequestering Mn^{2+}. Given that Mn^{2+} potentiates the antimicrobial innate immune response and that the Mn^{2+}-binding effector TssS was delivered into the cytosol of host cells via T6SS, we postulated that TssS could reduce free Mn^{2+} levels in the cytosol of host cells as a Mn^{2+} chelator, thereby suppressing host innate immunity. To test this hypothesis, we first treated PMs with TssS or the Mn^{2+} chelator ethylenediamine-*N*,*N*′-bis(2-hydroxyphenylacetic acid) (EDDHA). As expected, the addition of EDDHA to the culture medium dramatically reduced c-di-GMP–stimulated ISG expression (Fig. 6*A*). More importantly, defective ISG expression was strongly reversed with the addition of Mn^{2+}, confirming the notion that the host innate immune response could be suppressed by Mn^{2+} chelation. Similarly, the addition of apo-TssS protein to the culture medium substantially reduced c-di-GMP–stimulated ISG expression, and supplementation with Mn^{2+} effectively restored ISG expression (Fig. 6*A*). A recent study showed that Mn^{2+} promotes STING activation by enhancing 2′3′-cGAMP–STING affinity (13). Consistent with this, we found that Mn^{2+} enhanced the affinity of STING for c-di-GMP by 2.43-fold. As anticipated, the effect of Mn^{2+} on c-di-GMP/STING affinity was abrogated by supplementation of the apo-TssS protein but not TssS* protein (*SI Appendix*, Fig. S7*A*).

The role of TssS as a Mn^{2+} chelator was confirmed by testing its ability to inhibit cGAS activity. Consistent with previous reports (13, 43), the addition of Mn^{2+} strongly increased cGAS-mediated 2′3′-cGAMP production, and this effect was abrogated by the addition of EDDHA or other chelators such as ethylenediaminetetraacetic acid and diethylenetriaminepentaacetic acid (*SI Appendix*, Fig. S7*B*). Similarly, the addition of 10 μM TssS protein potently inhibited Mn^{2+}-activated cGAS enzymatic activity, but the TssS* mutant protein did not have this effect (Fig. 6 *B*, *Middle*). Moreover, TssS inhibits cGAS activity in a dose-dependent manner (Fig. 6 *B*, *Bottom*). As reported (13), the presence of Mg^{2+} supported cGAS activation in vitro, albeit less effectively than Mn^{2+} (*SI Appendix*, Fig. S7*C*). However, the TssS protein did not affect Mg^{2+}-induced cGAS activation but strongly inhibited Mn^{2+}-induced 2′3′-cGAMP production (*SI Appendix*, Fig. S7*C*), further confirming that TssS inhibits cGAS activity by sequestering Mn^{2+}. It is noteworthy that TssS did not interact with cGAS in an in vitro–binding assay (*SI Appendix*, Fig. S7*D*), thus ruling out the possibility that TssS inhibits cGAS activity by direct physical contact. Together, these results demonstrated that TssS inhibits cGAS-STING activity by chelating Mn^{2+}, an activator of the cGAS-STING pathway (13). Consistently, suppressing the cGAS-STING pathway by overexpressing TssS resulted in increased DNA virus infection as manifested by the higher titer of DNA virus vaccinia in HeLa cells (Fig. 6*C* and *SI Appendix*, Fig. S7*E*).

Finally, to verify whether TssS reduces the cytosolic free Mn^{2+} level in host cells by acting as an Mn^{2+} chelator, we measured the intracellular Mn^{2+} concentration after the addition of apo-TssS to the culture medium. The cytoplasmic Mn^{2+} concentration was markedly reduced by the addition of the apo-TssS protein but not the TssS* mutant protein (Fig. 6*D* and *SI Appendix*, Fig. S7*F*). Therefore, the Mn^{2+}-chelating micropeptide TssS inhibits cGAS-STING activation by sequestering immunostimulatory Mn^{2+}.

Discussion

Here, we show that a T6SS-secreted anti-eukaryotic effector, TssS, deploys a unique virulence strategy by sequestering immunostimulatory Mn^{2+} in the host cell to antagonize the STING-mediated innate immune response (Fig. 7). To the best of our knowledge, TssS is the smallest bacterial effector reported to date that is involved in bacterial pathogen–host interactions. Although TssS is a micropeptide of only 48 amino acids, it uses a multifaceted mechanism to promote bacterial virulence, involving competition for essential Mn^{2+}, resistance to oxidative stress, and suppression of the host immune response. Distinct from traditional bacterial effectors that are generally large proteins acting as enzymes, adaptors, and transcriptional activators (44–46), the micropeptide TssS conducts its functions simply but effectively by acting as a specific Mn^{2+} chelator.

Cellular ionic concentrations are central factors for orchestrating host innate immunity. For instance, intracellular potassium leakage inhibits the cGAS-STING-IFNβ cascade but triggers NLRP3 activation (47), abnormal intracellular calcium levels suppress the STING signaling pathway (48, 49), and an accumulation of Zn^{2+} in cytoplasm activates innate immunity by enhancing the enzymatic activity of cGAS (41, 50). We recently revealed that Mn^{2+} is vital to the innate immune response against DNA virus infection, as it potentiates the cGAS-STING pathway (13). Importantly, Mn^{2+} directly activates cGAS to produce 2′3′-cGAMP in a ligand binding–independent manner, and it also increases cGAMP-STING–binding affinity to potentiate STING activity, which are critical for antiviral and antitumor host responses (43, 51–53). In conjunction with these studies, we show here that Mn^{2+} enhanced the antimicrobial innate immune response and dramatically increased the survival rate of mice after *Yptb* infection (Fig. 4). Similar to that of Zn (41, 42), we found that the cytoplasmic level of Mn is strongly increased by LPS stimulation, indicating that *Yptb* infection may drive Mn release from membrane-enclosed organelles and thereby potentiate the cGAS-STING pathway (Fig. 4) (13, 36).

The finding that Mn^{2+} primes the STING-mediated innate immune response against *Yptb* infection is consistent with a previous report that in addition to the TLR-dependent innate immune response, a TLR-independent innate immune response was also induced against *Yptb* infection (54). When comparing the WT-infected C57BL/6 and STING-deficient mice, higher bacterial loads were obtained from the feces and cecum of STING-deficient mice (Fig. 4*E*), which signifies that the STING pathway plays weak but unambiguous roles in defending against *Yptb* infection. Thus, we speculated that the TLR-dependent pathway plays the major role, while the TLR-independent Mn^{2+}-STING pathway plays an auxiliary role in the stimulation of innate immunity upon sensing *Yptb* infection. Although the

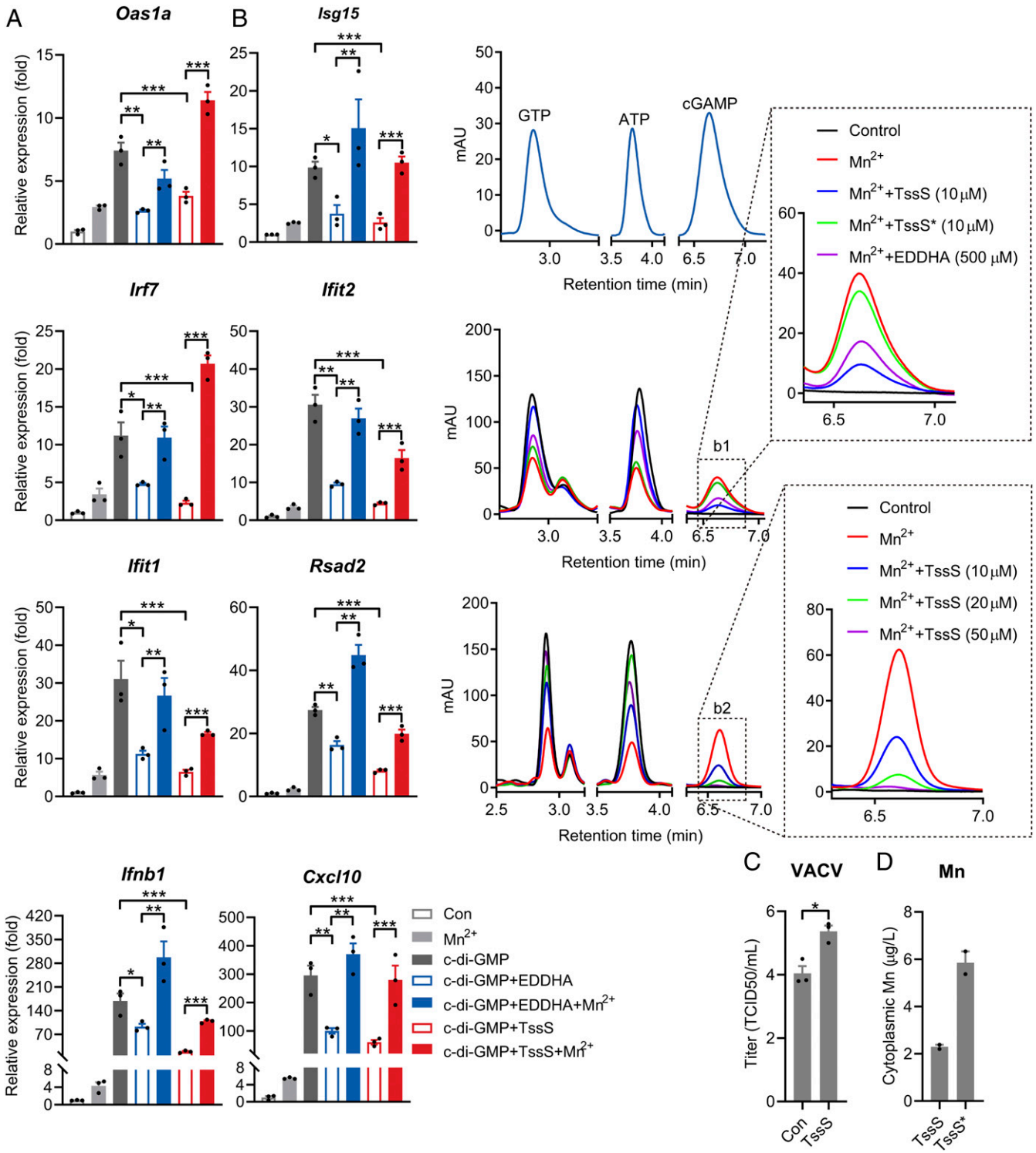

Fig. 6. TssS acts as a Mn^{2+} chelator to suppress STING-mediated innate immune response. (*A*) qRT-PCR analysis of gene expression in PMs untreated (Con) or pretreated with 10 μM TssS and 50 μM EDDHA along with or without 100 μM Mn^{2+} for 24 h and then transfected with 20 μM c-di-GMP for 4 h. (*B*) 2′3′-cGAMP production was measured by high-performance liquid chromatography. 2′3′-cGAMP was produced in the presence of 0.2 mM ATP and 0.2 mM GTP by cGAS under 10^{-2} mg · mL^{-1} double-stranded DNA. (*Middle*) Added without (Con) or with 1 mM Mn^{2+}, 10 μM TssS protein, 10 μM TssS* protein, or 500 μM EDDHA for 2 h. (*Bottom*) Added without (Con) or with 1 mM Mn^{2+} or the indicated concentrations of TssS protein for 2 h (as described in *Materials and Methods*). (*Insets*) Expanded views of the indicated products. (*C*) Viral titers in HeLa cells transduced with the pSIN-IRES-Puro-4×*tssS* overexpression vector. At 24 h post-transduction, the cells were infected with virus vaccinia at a multiplicity of infection of 0.01. Viral titers were determined at 24 h postinfection. (*D*) Mn concentrations in Raw264.7 cytoplasm. Raw264.7 was coincubated with TssS or TssS* protein (10 μM) for 30 min. The cytoplasmic Mn^{2+} concentration was measured by ICP-MS after removing His_6-tagged TssS or TssS* proteins with His•Bind Ni-NTA resin. Data in *A* were normalized to untreated, nontransfected control (Con, set as 1), and *Gapdh* was used as the housekeeping gene. Error bars represent ± SEM; $*P < 0.05$; $**P < 0.01$; $***P < 0.001$.

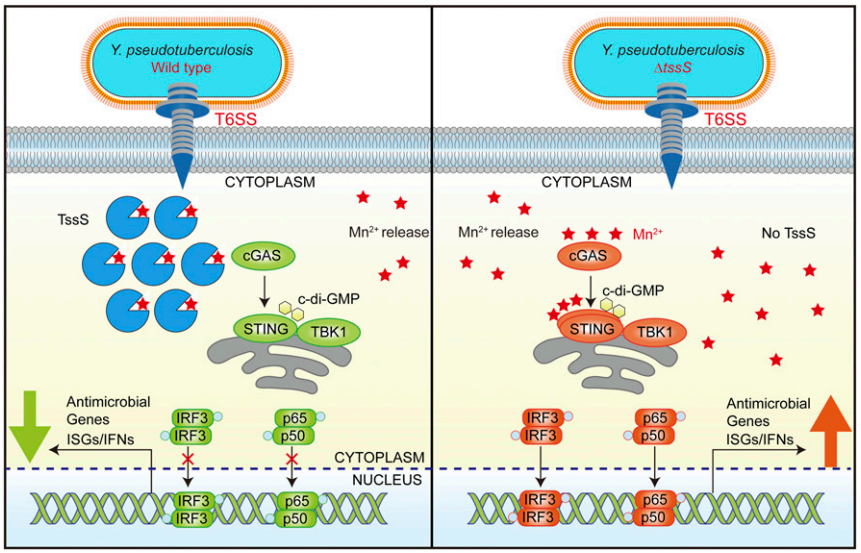

Fig. 7. Model of TssS-induced suppression of STING-mediated innate immunity. *Yptb* infection induces Mn^{2+} release from membrane-enclosed organelles into the cytosol of host cells, boosting activation of the cGAS-STING pathway. In host cells infected with *Yptb* WT (*Left*), the Mn^{2+}-chelating micropeptide TssS was translocated into the cytosol via its T6SS. TssS suppresses the Mn^{2+}-enhanced STING-mediated innate immune response by chelating Mn^{2+}, thus reducing bacterial clearance. When host cells were infected with the Δ*tssS* mutant (*Right*), no Mn^{2+}-chelating TssS was translocated, and the bioavailability of Mn^{2+} was higher. Consequently, STING and its downstream pathways were activated to a greater extent, restricting infection by the Δ*tssS* mutant.

spectrum of its antimicrobial activity requires further investigation, we envision that the Mn^{2+}-mediated innate immune system activation may be involved in diverse biological processes and could represent a new strategy for the development of therapeutic approaches to combat microbial infection.

Given the crucial roles of metal ions in regulating host innate immunity, it is reasonable to speculate that bacterial pathogens may manipulate the bioavailability of these ions to mediate host innate responses. As anticipated, we found that *Yptb* T6SS translocated TssS into host cells to inhibit the STING-mediated innate immune response by sequestering immunostimulatory Mn^{2+}. This finding is supported by at least four lines of evidence: 1) the transcriptomic analysis showed that the Δ*tssS* mutant elicited a significantly more intense innate immune response compared to *Yptb* WT infection, and many of the differentially expressed genes belonged to IFN- and STING-related signaling pathways (Fig. 2*A*); 2) in vitro experiments showed that TssS inhibited the Mn^{2+}-enhanced cGAS catalytic activity, STING oligomerization, and activation of downstream signaling pathways (Figs. 5*C* and 6*B*); 3) the bioavailability of Mn^{2+} in the cytosol of host cells was reduced by TssS (Fig. 6*D*); and 4) the function of STING was inhibited by TssS in vivo as illustrated by the lower bacterial burdens of the Δ*tssS* mutant potently increasing in STING-deficient mice (Fig. 5*E* and *SI Appendix*, Fig. S6 *C* and *D*). Indeed, the addition of apo-TssS (50 μM) potently reduced free Mn^{2+} concentration from 1 to 0. 4 mM in the Tris HCl buffer, indicating that one TssS molecule can bind roughly 12 Mn^{2+} ions (*SI Appendix*, Fig. S7*G*). Overall, we demonstrated an immune evasion strategy employed by *Yptb*, which modulates the cellular bioavailability of immunomodulatory metal ions using a metal-chelating T6SS effector. Interestingly, similar T6SS clusters containing putative Mn^{2+}-binding effectors have been identified in diverse bacteria strains (*SI Appendix*, Fig. S3), suggesting this T6SS-mediated Mn^{2+} sequestration mechanism might be employed by a broad range of pathogenic bacteria to suppress host innate immune responses.

Indeed, modulation of the bioavailability of metal ions is a successful host strategy to prevent infection, which is termed as nutritional immunity (55). To prevent bacterial access to essential metal ions, vertebrate hosts use a number of metal-chelating proteins such as ferritin, transferrin, and siderocalin to sequester Fe and calprotectin to sequester Mn and Zn (55). Remarkably, the 24-meric heteropolymers of ferritin have the ability to store up to several thousand iron atoms per protein (56). To battle for essential micronutrients, bacterial pathogens have developed sophisticated transport systems to uptake specific nutrient metals (54). Although it remains unclear whether the Mn^{2+}-chelating effector TssS is involved in combating calprotectin-mediated host nutritional immunity, we believe that reduction of the bioavailability of free metal ions in host cells by bacterial effectors may represent a universal immune evasion strategy employed by diverse pathogenic bacteria.

In summary, our results reveal a previously unrecognized mechanism of immune suppression involving sequestration of immunologically active metal ions (Fig. 7) and highlight the importance of micropeptides, which have been largely unexplored, in pathogen–host interactions. Considering that multiple T6SS effectors involved in the chelation of metal ions such as Mn, Zn, Fe, and Cu have been identified recently in various bacterial pathogens (10, 30, 57–59), the sequestration of metal ions by metal-chelating effectors may represent a unique and universal virulence strategy to perturb host immunity. Moreover, our identification of a STING-suppressing micropeptide may represent a novel strategy that can be applied to the development of treatments that prevent excessive innate immune activation as therapy for autoinflammatory diseases.

Materials and Methods

Bacterial Strains and Growth Conditions. Bacterial strains and plasmids used in this study are listed in *SI Appendix*, Table S1. Details are in *SI Appendix*.

Plasmid Construction. Primers used in this study are listed in *SI Appendix*, Table S2. Details are in *SI Appendix*.

Mouse Infection. Mice used in this study were on a C57BL/6 background. *Tmem173*$^{-/-}$ mice were generated in a previous work (13). All mouse experimental procedures were performed in accordance with the Regulations for the Administration of Affairs Concerning Experimental Animals approved by the State Council of People's Republic of China. For survival assays, 1×10^9 bacteria of each strain were applied to different groups of mice, and the survival rate of the mice was determined by monitoring the survival daily for 21 d (60). For the analysis of the bacterial load in the feces, the feces were sampled from individual living mice at specific time points, weighed, and homogenized in phosphate-buffered saline (PBS). For the analysis of the bacterial load in the cecum, colon, spleen, and liver, mice were euthanized by carbon dioxide asphyxiation followed with cervical dislocation at specific time points after infection, the tissue were weighed and homogenized in PBS, and serial dilutions of the homogenates were plated on YLB plates with 20 μg · mL^{-1} nalidixic acid. Details are in *SI Appendix*.

Cell Culture. Details are in *SI Appendix*.

Macrophage Infection. The cells were infected by *Yptb* strains at a multiplicity of infection of 20 or otherwise indicated (61). The plates were centrifuged at 500 *g* for 5 min to improve contact of bacteria with cells and subsequently incubated infected cells at 37 °C for 2 h, and antibiotics and isopropylthio-β-galactoside (IPTG) (1 mM) need to be added during this time when necessary. Then, the cells were washed by PBS two times and resuspended in medium with fetal bovine serum and penicillin/streptomycin and subsequently incubated at 37 °C with 5% CO_2 for 4 h. Cells were collected at 6 h postinfection. Then, the cells were collected for RNA isolation and immunoblotting. Details are in *SI Appendix*. All reagents and resources used in this study are listed in *SI Appendix*, Table S3.

Overexpression and Purification of Recombinant Protein. Details are in *SI Appendix*.

GST Pull-down Assay. The GST pull-down assay was performed as previously described with minor modifications (10, 62). Details are in *SI Appendix*.

Protein Secretion Assay. A secretion assay for TssS was performed according to described methods (63). Details are in *SI Appendix*.

Quantitative Real-Time PCR. qRT-PCR was performed in a CFX96 Real-Time PCR Detection System (Bio-Rad) with TransStart Green qPCR SuperMix (TransGen Biotech). The relative abundance of 16S ribosomal RNA was used as the internal standard in bacterial cells, and *Gapdh* was used as internal standard in mammalian cells. All samples were analyzed in triplicate, and the expression of target genes was calculated as relative fold values using the $2^{-\Delta\Delta Ct}$ method. Details are in *SI Appendix*. All primers for qRT-PCR were listed in *SI Appendix*, Table S2.

Western Blot Analysis. Samples were separated by sodium dodecyl sulfate–polyacrylamide gel electrophoresis and transferred onto polyvinylidene fluoride (PVDF) membranes (Millipore). The membrane was blocked with QuickBlock Blocking Buffer (Beyotime Biotechnology) for 30 min at room temperature and incubated with primary antibodies at 4 °C overnight. The membrane was washed three times in Tris buffered saline with Tween 20 (TBST) buffer (50 mM Tris, 150 mM NaCl, and 0.05% Tween 20, pH 7.4) and incubated with horseradish peroxidase–conjugated secondary antibodies for 1 h. Signals were detected using the ECL Kit (Invitrogen) following the manufacturer's specified protocol. Antibodies used are listed in *SI Appendix*, Table S3.

Bacterial Survival Assay. Details are in *SI Appendix*.

Measurement of Microelement by Inductively Coupled Plasma Mass Spectrometry. Bacterial intracellular ion content was determined as described previously (10, 30). Samples were analyzed by inductively coupled plasma mass spectrometry (ICP-MS, Varian 802-MS), and the results were corrected using the appropriate buffers for reference and dilution factors. For the intracellular ion in mammalian cells, the measurement of microelement by ICP-MS was performed as described with minor modifications (13). Details are in *SI Appendix*.

Metal-Free TssS Preparation and Metal Ion–Binding Assays. Details are in *SI Appendix*.

ITC. Mn^{2+} binding was measured using ITC at 25 °C as previously described with minor modifications with a NANO-ITC 2G microcalorimeter (TA Instruments) (64). Details are in *SI Appendix*.

Cya Assay. The Cya assay was performed as previously described with minor modifications (32). Details are in *SI Appendix*.

Translocation Assay for TssS::TEM1 Fusions. The translocation assay was performed as previously described (65). Details are in *SI Appendix*.

cGAS-cGAMP Activity Assay. The cGAS-cGAMP activity assay was analyzed as described previously with minor modifications (13). High-performance liquid chromatography was performed at a constant flow rate of 1.0 mL · min^{-1} with 98% (vol/vol) phase A and 2% (vol/vol) phase C. The UV absorption was measured at 254 nm, and the column temperature was maintained at 27 °C. Various nucleotide states, including ATP, GTP, and 2′3′-cGAMP, were used as standards to determine the retention times and amounts of the various ingredients in the reaction mixture. Details are in *SI Appendix*.

Transfection. Details are in *SI Appendix*.

Analyses of STING Oligomerization by Native Gels. The assay of the STING oligomers was analyzed as described previously with minor modifications (66). Details are in *SI Appendix*.

RNA-Seq Experiment. Details are in *SI Appendix*.

Diet-Induced Manganese Deficiency. Diet-induced manganese deficiency mice models were generated as described (13). Details are in *SI Appendix*.

Statistical Analysis. Experimental data analyzed for significance were performed by using GraphPad Prism 6 (GraphPad Software). *P* values for mice survival were calculated using log-rank (Mantel–Cox) test. *P* values for bacterial CFU in mouse tissues were calculated using Mann–Whitney *U* test (I). Statistical analyses for the rest of the assays were performed using paired two-tailed Student's *t* test. Error bars represent ± SEM; $*P < 0.05$; $**P < 0.01$; $***P < 0.001$.

Data Availability. All study data are included in the article and *SI Appendix*. Raw FASTQ files for the RNA-seq libraries are deposited in the National Center for Biotechnology Information Sequence Read Archive and have been assigned BioProject accession PRJNA635733.

ACKNOWLEDGMENTS. This work was supported by grants of the National Natural Science Foundation of China (Grants 31725003 and 31670053 to X.S., Grants 31970114 and 32170130 to Y.W., and Grant 31800113 to L.X.), National Key R&D Program of China (Grant 2018YFA0901200 to X.S.), the Open Project Program of the State Key Laboratory of Pathogen and Biosecurity (Grant SKLPBS1825 to X.S.), China Postdoctoral Science Foundation (Grant 2018M631201, to L.X. and Grant 2020M673501, to L.Z.), and Chinese Universities Scientific Fund (the Starting Research Fund from the Northwest A&F University, Grant 2452018045, to L.X.). L.X. is supported by the Shaanxi Postdoctoral Science Foundation (Grant 2018BSHTDZZ20) and the Natural Science Basis Research Plan in Shaanxi Province of China (Grant 2020JQ-245). We thank the Teaching and Research Core Facility at College of Life Science (Min Duan, Ningjuan Fan, Xiyan Chen, and Hui Duan) and Life Science Research Core Services, Northwest A&F University for the technical support.

1. A. B. Russell, S. B. Peterson, J. D. Mougous, Type VI secretion system effectors: Poisons with a purpose. *Nat. Rev. Microbiol.* **12**, 137–148 (2014).
2. A. Joshi *et al.*, Rules of engagement: The type VI secretion system in *Vibrio cholerae*. *Trends Microbiol.* **25**, 267–279 (2017).
3. R. D. Hood *et al.*, A type VI secretion system of *Pseudomonas aeruginosa* targets a toxin to bacteria. *Cell Host Microbe* **7**, 25–37 (2010).
4. S. Y. Ting *et al.*, Bifunctional immunity proteins protect bacteria against FtsZ-targeting ADP-ribosylating toxins. *Cell* **175**, 1380–1392.e14 (2018).
5. W. Zhao, F. Caro, W. Robins, J. J. Mekalanos, Antagonism toward the intestinal microbiota and its effect on *Vibrio cholerae* virulence. *Science* **359**, 210–213 (2018).
6. H. E. Ledvina *et al.*, A phosphatidylinositol 3-kinase effector alters phagosomal maturation to promote intracellular growth of *Francisella*. *Cell Host Microbe* **24**, 285–295.e8 (2018).
7. D. F. Aubert *et al.*, A *Burkholderia* type VI effector deamidates Rho GTPases to activate the Pyrin inflammasome and trigger inflammation. *Cell Host Microbe* **19**, 664–674 (2016).
8. A. T. Ma, J. J. Mekalanos, In vivo actin cross-linking induced by *Vibrio cholerae* type VI secretion system is associated with intestinal inflammation. *Proc. Natl. Acad. Sci. U.S.A.* **107**, 4365–4370 (2010).
9. H. Chen *et al.*, The bacterial T6SS effector EvpP prevents NLRP3 inflammasome activation by inhibiting the Ca^{2+}-dependent MAPK-Jnk pathway. *Cell Host Microbe* **21**, 47–58 (2017).
10. M. Si *et al.*, Manganese scavenging and oxidative stress response mediated by type VI secretion system in *Burkholderia thailandensis*. *Proc. Natl. Acad. Sci. U.S.A.* **114**, E2233–E2242 (2017).
11. J. D. Aguirre, V. C. Culotta, Battles with iron: Manganese in oxidative stress protection. *J. Biol. Chem.* **287**, 13541–13548 (2012).
12. V. E. Diaz-Ochoa *et al.*, *Salmonella* mitigates oxidative stress and thrives in the inflamed gut by evading calprotectin-mediated manganese sequestration. *Cell Host Microbe* **19**, 814–825 (2016).
13. C. Wang *et al.*, Manganese increases the sensitivity of the cGAS-STING pathway for double-stranded DNA and is required for the host defense against DNA viruses. *Immunity* **48**, 675–687.e7 (2018).
14. L. Sun, J. Wu, F. Du, X. Chen, Z. J. Chen, Cyclic GMP-AMP synthase is a cytosolic DNA sensor that activates the type I interferon pathway. *Science* **339**, 786–791 (2013).
15. D. Gao *et al.*, Cyclic GMP-AMP synthase is an innate immune sensor of HIV and other retroviruses. *Science* **341**, 903–906 (2013).
16. T. S. Xiao, K. A. Fitzgerald, The cGAS-STING pathway for DNA sensing. *Mol. Cell* **51**, 135–139 (2013).

17. Q. Chen, L. Sun, Z. J. Chen, Regulation and function of the cGAS-STING pathway of cytosolic DNA sensing. *Nat. Immunol.* **17**, 1142–1149 (2016).
18. D. L. Burdette *et al.*, STING is a direct innate immune sensor of cyclic di-GMP. *Nature* **478**, 515–518 (2011).
19. J. D. Sauer *et al.*, The *N*-ethyl-*N*-nitrosourea-induced *Goldenticket* mouse mutant reveals an essential function of *Sting* in the in vivo interferon response to *Listeria monocytogenes* and cyclic dinucleotides. *Infect. Immun.* **79**, 688–694 (2011).
20. X. Zhang *et al.*, Cyclic GMP-AMP containing mixed phosphodiester linkages is an endogenous high-affinity ligand for STING. *Mol. Cell* **51**, 226–235 (2013).
21. K. P. Hopfner, V. Hornung, Molecular mechanisms and cellular functions of cGAS-STING signalling. *Nat. Rev. Mol. Cell Biol.* **21**, 501–521 (2020).
22. A. F. U. H. Saeed, X. Ruan, H. Guan, J. Su, S. Ouyang, Regulation of cGAS-mediated immune responses and immunotherapy. *Adv. Sci. (Weinh.)* **7**, 1902599 (2020).
23. J. Kwon, S. F. Bakhoum, The cytosolic DNA-sensing cGAS-STING pathway in cancer. *Cancer Discov.* **10**, 26–39 (2020).
24. F. V. Marinho, S. Benmerzoug, S. C. Oliveira, B. Ryffel, V. F. J. Quesniaux, The emerging roles of STING in bacterial infections. *Trends Microbiol.* **25**, 906–918 (2017).
25. L. K. Chung *et al.*, The *Yersinia* virulence factor YopM Hijacks host kinases to inhibit type III effector-triggered activation of the Pyrin inflammasome. *Cell Host Microbe* **20**, 296–306 (2016).
26. U. Meinzer *et al.*, *Yersinia pseudotuberculosis* effector YopJ subverts the Nod2/RICK/TAK1 pathway and activates caspase-1 to induce intestinal barrier dysfunction. *Cell Host Microbe* **11**, 337–351 (2012).
27. G. I. Viboud, J. B. Bliska, *Yersinia* outer proteins: Role in modulation of host cell signaling responses and pathogenesis. *Annu. Rev. Microbiol.* **59**, 69–89 (2005).
28. L. Song *et al.*, Contact-independent killing mediated by a T6SS effector with intrinsic cell-entry properties. *Nat. Commun.* **12**, 423 (2021).
29. W. Zhang *et al.*, A type VI secretion system regulated by OmpR in *Yersinia pseudotuberculosis* functions to maintain intracellular pH homeostasis. *Environ. Microbiol.* **15**, 557–569 (2013).
30. T. Wang *et al.*, Type VI secretion system transports Zn^{2+} to combat multiple stresses and host immunity. *PLoS Pathog.* **11**, e1005020 (2015).
31. J. M. Silverman *et al.*, Haemolysin coregulated protein is an exported receptor and chaperone of type VI secretion substrates. *Mol. Cell* **51**, 584–593 (2013).
32. H. Nagai *et al.*, A C-terminal translocation signal required for Dot/Icm-dependent delivery of the *Legionella* RalF protein to host cells. *Proc. Natl. Acad. Sci. U.S.A.* **102**, 826–831 (2005).
33. E. Vigonsky *et al.*, Metal binding spectrum and model structure of the *Bacillus anthracis* virulence determinant MntA. *Metallomics* **7**, 1407–1419 (2015).
34. M. Lu, D. Fu, Structure of the zinc transporter YiiP. *Science* **317**, 1746–1748 (2007).
35. J. E. Martin, D. P. Giedroc, Functional determinants of metal ion transport and selectivity in paralogous cation diffusion facilitator transporters CzcD and MntE in *Streptococcus pneumoniae. J. Bacteriol.* **198**, 1066–1076 (2016).
36. A. Carmona, S. Roudeau, L. Perrin, G. Veronesi, R. Ortega, Environmental manganese compounds accumulate as Mn(II) within the Golgi apparatus of dopamine cells: Relationship between speciation, subcellular distribution, and cytotoxicity. *Metallomics* **6**, 822–832 (2014).
37. C. Aude-Garcia *et al.*, Different in vitro exposure regimens of murine primary macrophages to silver nanoparticles induce different fates of nanoparticles and different toxicological and functional consequences. *Nanotoxicology* **10**, 586–596 (2016).
38. Y. C. Kim *et al.*, Simvastatin induces caspase-independent apoptosis in LPS-activated RAW264.7 macrophage cells. *Biochem. Biophys. Res. Commun.* **339**, 1007–1014 (2006).
39. U. C. Yadav, N. M. Kalariya, S. K. Srivastava, K. V. Ramana, Protective role of benfotiamine, a fat-soluble vitamin B1 analogue, in lipopolysaccharide-induced cytotoxic signals in murine macrophages. *Free Radic. Biol. Med.* **48**, 1423–1434 (2010).
40. T. E. Gunter, K. K. Gunter, J. S. Puskin, P. R. Russell, Efflux of Ca^{2+} and Mn^{2+} from rat liver mitochondria. *Biochemistry* **17**, 339–345 (1978).
41. R. Kapetanovic *et al.*, *Salmonella* employs multiple mechanisms to subvert the TLR-inducible zinc-mediated antimicrobial response of human macrophages. *FASEB J.* **30**, 1901–1912 (2016).
42. H. Haase *et al.*, Zinc signals are essential for lipopolysaccharide-induced signal transduction in monocytes. *J. Immunol.* **181**, 6491–6502 (2008).
43. R. M. Hooy, G. Massaccesi, K. E. Rousseau, M. A. Chattergoon, J. Sohn, Allosteric coupling between Mn^{2+} and dsDNA controls the catalytic efficiency and fidelity of cGAS. *Nucleic Acids Res.* **48**, 4435–4447 (2020).
44. S. Kay, S. Hahn, E. Marois, G. Hause, U. Bonas, A bacterial effector acts as a plant transcription factor and induces a cell size regulator. *Science* **318**, 648–651 (2007).
45. M. P. Müller *et al.*, The *Legionella* effector protein DrrA AMPylates the membrane traffic regulator Rab1b. *Science* **329**, 946–949 (2010).
46. Y. Xu *et al.*, A bacterial effector reveals the V-ATPase-ATG16L1 axis that initiates xenophagy. *Cell* **178**, 552–566.e20 (2019).
47. I. Banerjee *et al.*, Gasdermin D restrains type I interferon response to cytosolic DNA by disrupting ionic homeostasis. *Immunity* **49**, 413–426.e5 (2018).
48. D. Kwon, H. Sesaki, S. J. Kang, Intracellular calcium is a rheostat for the STING signaling pathway. *Biochem. Biophys. Res. Commun.* **500**, 497–503 (2018).
49. S. Srikanth *et al.*, The Ca^{2+} sensor STIM1 regulates the type I interferon response by retaining the signaling adaptor STING at the endoplasmic reticulum. *Nat. Immunol.* **20**, 152–162 (2019).
50. M. Du, Z. J. Chen, DNA-induced liquid phase condensation of cGAS activates innate immune signaling. *Science* **361**, 704–709 (2018).
51. L. Hou *et al.*, Manganese-based nanoactivator optimizes cancer immunotherapy via enhancing innate Immunity. *ACS Nano* **14**, 3927–3940 (2020).
52. Z. Zhao *et al.*, Mn(2+) directly activates cGAS and structural analysis suggests Mn(2+) induces a noncanonical catalytic synthesis of 2′3′-cGAMP. *Cell Rep.* **32**, 108053 (2020).
53. M. Lv *et al.*, Manganese is critical for antitumor immune responses via cGAS-STING and improves the efficacy of clinical immunotherapy. *Cell Res.* **30**, 966–979 (2020).
54. V. Auerbuch, D. T. Golenbock, R. R. Isberg, Innate immune recognition of *Yersinia pseudotuberculosis* type III secretion. *PLoS Pathog.* **5**, e1000686 (2009).
55. M. I. Hood, E. P. Skaar, Nutritional immunity: Transition metals at the pathogen-host interface. *Nat. Rev. Microbiol.* **10**, 525–537 (2012).
56. J. M. Bradley *et al.*, Bacterial iron detoxification at the molecular level. *J. Biol. Chem.* **295**, 17602–17623 (2020).
57. J. Lin *et al.*, A *Pseudomonas* T6SS effector recruits PQS-containing outer membrane vesicles for iron acquisition. *Nat. Commun.* **8**, 14888 (2017).
58. Y. Han *et al.*, A *Pseudomonas aeruginosa* type VI secretion system regulated by CueR facilitates copper acquisition. *PLoS Pathog.* **15**, e1008198 (2019).
59. C. Li *et al.*, T6SS secretes an LPS-binding effector to recruit OMVs for exploitative competition and horizontal gene transfer. *ISME J.* 10.1038/s41396-021-01093-8. (2021).
60. J. Schweer *et al.*, The cytotoxic necrotizing factor of *Yersinia pseudotuberculosis* (CNFY) enhances inflammation and Yop delivery during infection by activation of Rho GTPases. *PLoS Pathog.* **9**, e1003746 (2013).
61. T. J. Schoberle, L. K. Chung, J. B. McPhee, B. Bogin, J. B. Bliska, Uncovering an important role for YopJ in the inhibition of caspase-1 in activated macrophages and promoting *Yersinia pseudotuberculosis* virulence. *Infect. Immun.* **84**, 1062–1072 (2016).
62. X. Shen *et al.*, Targeting eEF1A by a *Legionella pneumophila* effector leads to inhibition of protein synthesis and induction of host stress response. *Cell. Microbiol.* **11**, 911–926 (2009).
63. S. Xu *et al.*, FliS modulates FlgM activity by acting as a non-canonical chaperone to control late flagellar gene expression, motility and biofilm formation in *Yersinia pseudotuberculosis. Environ. Microbiol.* **16**, 1090–1104 (2014).
64. L. Zhang *et al.*, Sensing of autoinducer-2 by functionally distinct receptors in prokaryotes. *Nat. Commun.* **11**, 5371 (2020).
65. F. Jiang, N. R. Waterfield, J. Yang, G. Yang, Q. Jin, A *Pseudomonas aeruginosa* type VI secretion phospholipase D effector targets both prokaryotic and eukaryotic cells. *Cell Host Microbe* **15**, 600–610 (2014).
66. C. Zhang *et al.*, Structural basis of STING binding with and phosphorylation by TBK1. *Nature* **567**, 394–398 (2019).